The Astrophysical Journal, 987:17 (16pp), 2025 July 1 https://doi.org/10.3847/1538-4357/add938
© 2025. The Author(s). Published by the American Astronomical Society.
OPEN ACCESS

Evaluating the Effects of Thermal Processing on Nucleosynthetic Zinc Isotope Variations: Insights from Carbonaceous Chondrites Leachates

Rayssa Martins[1,2], Elin M. Morton[1], Alessandro Bragagni[3,4], Helen M. Williams[2], Frank Wombacher[4], and Mark Rehkämper[1]
[1] Department of Earth Sciences and Engineering, Imperial College London, South Kensington Campus, London, SW7 2AZ, UK; rm2185@cam.ac.uk
[2] Department of Earth Sciences, University of Cambridge, Downing Street, Cambridge, CB2 3EA, UK
[3] Consiglio Nazionale delle Ricerche, Istituto di Scienze Marine, via Gobetti 101, 40129 Bologna, Italy
[4] Universität zu Köln, Institut für Geologie und Mineralogie, 50674 Köln, Germany
Received 2024 December 12; revised 2025 May 5; accepted 2025 May 13; published 2025 June 24

Abstract

Variations in the nucleosynthetic isotope compositions of meteorites have been suggested to result from variable destruction of some presolar grains through thermal processing. This mechanism has furthermore been linked to volatile depletion in chondritic meteorites. As a moderately volatile element with variable nucleosynthetic isotope compositions, Zn potentially records both processes. Here, we present the nucleosynthetic Zn isotope compositions of leachates that target distinct mineral phases from four carbonaceous chondrites (CCs). The isotopic similarities between some leaching steps imply that different phases were partially homogenized, obscuring the original hosts of the neutron-rich (NR) Zn component that characterizes CCs. However, some leachates of the most primitive sample, Murchison CM2, display distinct Zn isotope compositions. The results reveal that the NR Zn was possibly hosted in silicate or oxide grains, which are similar or identical to the carriers of the bulk of the Zn. Multiple scenarios that simulate preferential Zn loss from such phases were modelled and compared to estimated compositions of thermally processed components in chondrites. The modelling suggests that variable extents of Zn depletion cannot account for the observed variations in nucleosynthetic Zn isotope compositions, implying that these characteristics are decoupled. Instead, distinct isotope compositions are required for the different Zn carriers depending on the chondrite group. The results thus suggest that thermal processing alone is not responsible for the observed nucleosynthetic Zn isotope variations. Rather, they most likely reflect temporal or spatial changes in the composition of the molecular cloud as the protoplanetary disk evolved, in line with other studies.

Unified Astronomy Thesaurus concepts: Meteorites (1038); Chondrites (228); Isotope shifts (2069); Mass spectrometry (2094); Carbonaceous chondrites (200); Solar system (1528)

1. Introduction

The elemental and isotopic compositions of solar system bodies were mainly inherited from nuclides produced during stellar nucleosynthesis (M. Lugaro 2005; A. Heger et al. 2014; T. Yokoyama & T. Tsujimoto 2021). This includes the atoms forged in stellar interiors, as well as nuclides assembled in the explosive events associated with their deaths, all of which can produce gas and dust with distinct elemental and isotopic abundances. Some presolar dust grains that inherit their composition from specific stellar sources were distributed in varying amounts throughout the solar system, imparting their distinct isotopic signatures onto the bodies that incorporated them.

These small variations in isotope compositions suggest the presence of two or more distinct reservoirs within the solar system (P. H. Warren 2011; M. Rüfenacht et al. 2023). Carbonaceous meteorites, from parent bodies that are thought to have accreted beyond the orbit of Jupiter (T. S. Kruijer et al. 2017), are generally enriched in isotopes that are produced in explosive nucleosynthesis. These include the neutron-rich (NR) isotopes of Ca, Ti, Cr, Ni, and Zn (A. Trinquier et al. 2007, 2009; N. Dauphas et al. 2014; J. A. M. Nanne et al. 2019; R. Martins et al. 2023), which are produced in either Type Ia (SN Ia) or Type II (SN II) supernovae, and the *r*-process isotopes of heavier elements like Mo, Ru, Sr, Zr, and Nd (L. Qin et al. 2011; W. Akram et al. 2015; T. Yokoyama et al. 2015; M. Fischer-Gödde & T. Kleine 2017; G. Budde et al. 2019). In contrast, noncarbonaceous (NC) meteorites and terrestrial planets, which formed in the inner solar system, are depleted in the same isotopes relative to carbonaceous meteorites.

The cause of the heterogenous distribution of this presolar dust is debated. Traditionally, it has been attributed to physical processes such as grain size sorting or thermal processing, which would have preferentially destroyed some presolar grains in the inner solar system (A. Trinquier et al. 2009; T. Yokoyama et al. 2015; M. Ek et al. 2020). This process has also been linked to primary volatile loss in the precursor materials that formed chondritic bodies (G. R. Huss et al. 2003). Alternatively, it has been suggested that this isotopic dichotomy reflects temporal and/or spatial changes in the composition of the infalling material from the molecular cloud as the protoplanetary disk was shaped (N. Dauphas et al. 2002; J. A. M. Nanne et al. 2019). In contrast to the first scenario, the latter model implies that the carrier phases of the anomalous material were never homogeneously distributed in the solar system. Notably, both hypotheses can account for the observed complementarity between the carbonaceous and NC reservoirs, as well as variations within each reservoir, making it difficult to favor one over the other.

Original content from this work may be used under the terms of the Creative Commons Attribution 4.0 licence. Any further distribution of this work must maintain attribution to the author(s) and the title of the work, journal citation and DOI.

Table 1
Chondrite Samples, Sample Weights, and Sources of the Meteorite Samples

Sample	Classification	Mass (g)	Supplier
Allende	CV3	4.505	Private Collector
Kainsaz	CO3.2	4.508	Russian Academy of Sciences
Colony	CO3.0 (desert find)	4.495	Smithsonian Institution
Murchison	CM2	4.502	Smithsonian Institution

A potential route to test the feasibility of the thermal processing scenario is to investigate the carrier phases responsible for the isotope anomalies and their thermal susceptibilities. Nucleosynthetic isotope anomalies of several elements, including Ti, Cr, Sr, Zr, Mo, and Pd, were previously interpreted as resulting from thermal processing (A. Trinquier et al. 2009; W. Akram et al. 2015; C. Burkhardt & M. Schönbächler 2015; T. Yokoyama et al. 2015; M. Ek et al. 2020). However, due to their relatively high condensation temperatures (K. Lodders 2003), these elements are not particularly sensitive to thermal perturbations and evaporation. As a moderately volatile element showcasing substantially variable elemental depletions across different meteorites and planets (J. T. Wasson & G. W. Kallemeyn 1988; H. S. C. O'Neill 1991; G. J. Taylor 2013; N. Braukmüller et al. 2018), Zn is an ideal candidate to test potential links between thermal processing and Zn loss, and the heterogenous distribution of presolar Zn carriers.

Previous leaching studies of the nucleosynthetic isotope anomalies determined for refractory elements show that some leachate steps display substantially larger anomalies than the bulk meteorites (e.g., A. Trinquier et al. 2009; C. Burkhardt & M. Schönbächler 2015). This method targets progressively more acid-resistant phases with each leaching step, such that the compositions of different minerals or mineral groups can be distinguished, thereby providing clues to the carrier phases of the isotope anomalies. Yet, while recent studies have characterized nucleosynthetic Zn isotope anomalies in a range of meteorites (P. S. Savage et al. 2022; T. Steller et al. 2022; R. Martins et al. 2023, 2024), the hosts of the Zn isotope anomalies are still unknown. Thus, the aim of this study is to characterize the mass-independent Zn isotope compositions of the distinct mineral phases present in carbonaceous chondrites (CCs), by performing a stepwise acid-leaching procedure.

2. Samples and Methods

2.1. Sample Preparation and Leaching Procedure

The initial sample preparation was performed at the University of Cologne. Four CC, including one CV, one CM, and two COs (Table 1), were crushed and about 4.5 g of the powder were subjected to a seven-step leaching procedure slightly modified from that of M. Rotaru et al. (1992) and C. Burkhardt & M. Schönbächler (2015). The reagents, their respective molarities, and volumes, as well as the durations, temperatures, and target phases of each step are summarized in Table 2, with the leachates shown in Figure 1. In the first step, the powdered samples were placed in standard 30 ml Savillex PFA vials and treated with the respective reagent. After leaching was completed, the vials with the mixtures of sample residues and leachates were centrifuged for 10–30 minutes, and the liquid fractions were pipetted to a new beaker. Next, the undigested residual fractions were rinsed with dilute acids (Table 2), and the rinses were added to the beakers containing the dissolved fractions. At this point, ~2% aliquots were separated from the dissolved fractions for elemental analysis. Finally, the contents of the beakers containing the dissolved and the undigested fractions were dried down at 80°C, and the residues in the latter were then treated with the subsequent leaching reagent.

This process was repeated until the seventh and final step, which encompasses five stages. In the first stage (7-a), the undigested residues were treated with the same reagents as in Step 6, but for this step, the samples were heated in Parr pressure digestion vessels for 3 days at 180°C. After centrifuging, the supernatants were transferred to the Step 7 beakers. Since undigested solids still remained, likely including graphite and fluoride compounds, the residues were dried down, and refluxed in an HCl–HNO_3 mix at 130°C for 1 day (7-b). The resulting liquid fractions were transferred to the Step 7 beakers, and the residues were dried down again. Next, the residues were refluxed in a Parr bomb with 2 ml 14.5 M HNO_3 at 180°C for one day, after which the liquid fractions were also transferred to the Step 7 beakers (7-c). The remaining solids were rinsed with 1.4 M HNO_3 and then treated twice with 8 M HCl at 55°C and 120°C for a day each (7-d; 7-e). The rinses were added to the Step 7 beakers, and the residues were dried down in between each rinse. Finally, the seven fractions obtained from each meteorite (Table 2) were dried and redissolved in 15 ml 1 M HCl ahead of the Zn separation procedure.

2.2. Zn Purification

Two initial stages of Zn separation were performed at the Institute for Geology and Mineralogy at the University of Cologne as part of an Sn separation procedure described in detail by A. Bragagni et al. (2023). The first stage employed 200–400 mesh Bio-Rad AG-1X8 anion-exchange resin in Bio-Rad columns with 2 ml resin beds (Table 3(a)). Zinc was eluted along with Sn using 1 M HNO_3. The Sn–Zn fractions were dried down and treated twice with 0.1 ml of a 30% H_2O_2, 15 M HNO_3, and 28 M HF mixture (5:10:1) to attack organics eluted from the resin. These solutions were again dried and redissolved in 2 ml 2 M HCl ahead of the second separation stage (Table 3(b)). This stage employed 0.8 ml of Triskem tributyl phosphate (TBP) resin and 0.4 ml of Triskem pre-filter material, which were loaded into custom columns made from PE pasteur pipettes. After loading the samples, Zn was eluted in 10 ml of 2 M HCl, which was collected in Savillex beakers and dried down.

Further processing of the Zn cuts, using the three-stage Zn anion-exchange procedure described in detail in R. Martins et al. (2023), was carried out at the MAGIC Laboratories at the Department of Earth Science & Engineering of Imperial College London. These three stages employed Teflon columns with 250 μl resin beds. Stage one used AG-1X8 100–200 mesh resin, and samples were loaded in 2 ml 3 M HCl. After the matrix elution steps, Zn was collected in 3 ml of a 0.1 M HBr + 0.5 M HNO_3 mix (R. Martins et al. 2023). The samples were then dried at 80°C and redissolved in 2 ml 1 M HCl. Next, they were loaded onto columns containing AG-MP1 100–200 mesh resin for both stages 2 and 3. Following loading of the sample solutions and matrix elution, Zn was eluted in 7 ml 0.01 M



Figure 1. Photograph showing the leachates obtained in leaching steps 1 through 6 (from left to right) in large beaker and the dissolved + residual fractions of Step 7 in small beakers after drying down. From top to bottom: Allende, Kainsaz, Colony, and Murchison.

Table 2
Summary of the Leaching Procedure

Step	Reagents	Molarity	Volume (ml)	Temp.	Time (days)	Rinse
1	Acetic acid	8.5 M	22	RT	1	MQ
2	HNO_3	4 M	18	RT	5	15 ml 0.14M HNO_3
3	HCl	6 M	18	80°C	1	15 ml 0.1M HCl
4	HCl–HF	3 M–12 M	20	100°C	6	15 ml 0.1M HCl
5	HCl–HF	3 M–12 M	20	160°C	2	15 ml 0.1M HCl
6	HNO_3–HF	7 M–12 M	8	160°C	1	no rinse
7-a	HNO_3–HF	7 M–12 M	8	180°C[a]	3	no rinse
7-b	HCl–HNO_3	6 M–3 M	5	130°C	1	no rinse
7-c	HNO_3	14.5 M	2	180°C[a]	1	5 ml 1.4M HNO_3
7-d	HCl	8 M	4	55°C	1	no rinse
7-e	HCl	8 M	5	120°C	1	no rinse

Notes. RT: room temperature.
[a] This step involved use of Parr pressure digestion vessels.

HCl. Finally, the samples were dried and redissolved in 0.1 M HNO_3 ahead of the isotope analyses.

2.3. Mass Spectrometry

Elemental analyses were performed on the 2% sample solution aliquots separated prior to the Zn separation procedure. This was done using a ThermoScientific iCAP Q inductively coupled plasma mass spectrometer (ICP-MS) in combination with a PFA nebulizer and spray chamber at the University of Cologne. The background signal was monitored during each analytical session by repeated measurements of a 2% HNO_3 solution and subtracted from the sample signals. Elemental mass fractions were calculated only when sample signals were above the average background level + 3SD of its variation. The results for each leaching step are reported as relative mass fractions of a given element in percent.

The isotope measurements were performed with a Nu Instruments Nu Plasma II multiple collector (MC-)ICP-MS at the MAGIC Laboratories following the procedure described in R. Martins et al. (2023). A Nu Instruments DSN 100 desolvation system fitted with glass cross flow nebulizers with solution flow rates of about 120 μl minute^{-1} were employed for sample introduction in conjunction with a CETAC ASX-112FR autosampler. The two Faraday cup configurations that were employed for the isotope measurements, with all cups connected to 10^{11} Ω resistors, are summarized in Table 4. The configurations were applied over separate sessions. Each run was started by a peak centering routine, while each block commenced with a 60 s measurement of the electronic baselines of the Faraday collectors while the ion beam was deflected in the electrostatic analyzer. The runs typically encompassed three blocks with 20 data acquisition cycles of 8 s each, however, samples with low Zn

Table 3
Zn Separation Procedure at the University of Cologne

(a) Stage I		
Reagent	Volume (ml)	Step
AG1X8 100–200 mesh	2	Add resin
1 M HCl	15	Load sample
1 M HCl	10	Elute matrix
1 M HCl	5	…
0.5 M HCl	5	…
0.5 M HCl	5	…
1 M HNO_3	5 × 4.7	Elute Sn and Zn
10 M HCl	2 × 7	Collect PGE
12 M HNO_3	2 × 7	…
(b) Stage II		
TBP resin/pre-filter	0.8/0.4	Add resin
2 M HCl	2	Load sample/Collect Zn
2 M HCl	1+4+2+2+1	Collect Zn

contents (<3 μg) were measured for two blocks of 20 measurements per repeat.

Monitoring of ^{73}Ge on the H10 Faraday cup during M70 block measurements (Table 4) revealed that Ge was consistently below the detection level. As such, no Ge corrections were needed, and the ion beam collected in Faraday cup H8 of the M64 block analyses was attributed exclusively to ^{70}Zn. Hence, provided that the H8 beam was sufficiently high (typically >0.4V) and stable, ε^{70}Zn values collected in M64 block measurements are also reported for some samples, such as Murchison (Steps 5–7), Allende (Steps 3–5), and Kainsaz (Steps 1–5, 7).

The sample solutions were introduced in 0.1 M HNO_3, typically containing 300–450 ng g^{-1} of Zn, with instrumental sensitivity ranging between 150 and 250 V $(\mu g\,ml^{-1})^{-1}$. All analyses were carried out with the sample—standard bracketing technique, in which sample runs were symmetrically bracketed by runs of the London Zn isotope reference material. Sample Zn concentrations typically matched the standard Zn concentrations to within 10%–15%.

The isotope results are reported using the ε-notation, which denotes deviations of the measured isotope ratio for a sample (sam) from the value determined for the London Zn reference standard (std) in parts per 10^4:

$$\varepsilon^{i}\mathrm{Zn} = \left(\frac{(^{i}\mathrm{Zn}/^{67}\mathrm{Zn})_{\mathrm{sam}}}{(^{i}\mathrm{Zn}/^{67}\mathrm{Zn})_{\mathrm{std}}} - 1\right) \times 10^4 \quad (1)$$

where i is the isotope of interest. Results employing both the ^{66}Zn/^{67}Zn and ^{64}Zn/^{67}Zn isotope ratios for internal normalization are reported. Since the ^{66}Zn/^{67}Zn normalization allows for monitoring of all five Zn isotopes and their isobaric interferences (R. Martins et al. 2023), this normalization is preferred and primarily adopted in the discussion, unless specified. The notation ε^{i}Zn is henceforth used to refer to results employing this normalization. In contrast, an $\varepsilon^{i}\mathrm{Zn}_{67/64}$ notation is employed for results obtained with internal normalization to ^{64}Zn/^{67}Zn.

The reported uncertainty formats vary depending on the number of runs that were carried out for a given sample. If only one run was performed, the uncertainty corresponds to twice the standard error of the mean (2SE) of the 40 or 60 individual 8 s measurements cycles performed in that run. If two or three runs were performed, the uncertainty corresponds the largest 2SE of the two or three runs. Finally, if more than three runs were performed, the uncertainty is equivalent to the 2SE of the means of all repeats.

For quality control, and to ensure the results are consistent with previous studies, the US Geological Survey reference material Columbia River Basalt, BCR-2, was regularly processed and analyzed along with the leachate samples, resulting in values that are consistent with previously published results and indistinguishable from the London Zn standard (R. Martins et al. 2023; Table 6). The blanks of the leaching procedure typically corresponded to <1% of the native sample Zn, with a minimum of 0.02% and a maximum of 5.8%. Assuming a terrestrial composition ($\varepsilon^{i}\mathrm{Zn} = 0$), the effect of the blanks on the isotope compositions of each sample can be estimated by mass balance. The average magnitude of these effects was ±0.01, ±0.00, and ±0.01 for ε^{64}Zn, ε^{68}Zn, and ε^{70}Zn, respectively, with a maximum of ±0.07, ±0.01, and ±0.15, which is within the precision of the measurements. Furthermore, the Zn separation procedure habitually yielded Zn blanks of <20 ng, which typically corresponds to between 0.1% and 2% of the indigenous Zn in the processed samples. Hence, no subsequent blank corrections were performed for the isotope results.

3. Results

3.1. Elemental Analyses

The results of the elemental analyses are reported as the element mass fractions released in each leaching step relative to the bulk elemental content (Table 5; Figure 2). For all four meteorites, most of the elements were leached in the first four steps, with Steps 5–7 yielding relatively small elemental fractions (Figure 1). Allende and Kainsaz display similar compositions for all leaching steps. In detail, Steps 1 and 2 (acetic acid and HNO_3, respectively) for these two meteorites released most of the Na (87%–95%), Mg (75%–87%), Al (54%–77%), P (93%–94%), K (97%–100%), Mn (61%–82%), Fe (90%–91%), Ni (94%–97%), and Cu (93%–96%). These first two steps also leached substantial S (35%–59%), Ca (29%–39%), and Ti (13%–17%), but only limited Zn (8%–10%). Step 3 (HCl) contains primarily Al (10%–15%), S (21%–24%), Ca (20%–24%), and Ti (23%–35%), with smaller fractions of Mg, P, Cr, Mn, Fe, Ni, Cu, and Zn (5%–8%). The first HF step, Step 4 (HCl–HF), released Ca (13%–39%), Ti (51%–57%), Cr (59%–70%), Mn (12%–32%), and Zn (78%–81%), but also some Na, Al, P, S, K, and Fe (<1%–4%). Albeit in much smaller amounts, Step 5 (HCl–HF) contains almost all of the same elements as Step 4, including Ca (1%), Ti (1%), Cr (9%–18%), Mn (1%), and Zn (2%–6%), as well as limited Na, Al, S, and K (<1%–2%). Step 6 (HNO_3–HF) is dominated by S (19%–42%), with small fractions of Cr (3%–5%), and Zn (<1%). Finally, Step 7 contains significant amounts of Al (11%–26%), and Ca (10%–23%), as well as smaller fractions of Na, Mg, Cr (<1%–7%), and very limited Zn (up to 1%).

Colony has some marked differences from Allende and Kainsaz. For instance, some of the elements that are released primarily in Steps 1 and 2 for Allende and Kainsaz, are released later in Colony. In detail, substantial fractions of P, Fe, Ni, and Cu are released in Step 3 (41%–59%), while much smaller fractions of these elements were leached in this step

Table 4
Collector Configurations That Were Used for the Zn Isotope Measurements, Abundances of the Isotopes of Zn, as Well as Spectral Interferences from Isobars and Ba^{2+}

Faraday Collector	L4	L2	Ax	H1	H2	H4	H6	H7	H8	H10
Collector Configuration M64	^{62}Ni	^{64}Zn	…	…	^{66}Zn	^{67}Zn	^{68}Zn	$^{137}Ba^{2+}$	^{70}Zn	…
Isotope Abundance Zn	…	49.2	…	…	27.7	0	18.5	…	0.6	…
Isotope abundance Ni	3.6	0.1	…	…	…	…	…	…	…	…
Isotope Abundance Ba^{2+} ions	…	…	…	…	0.1	2.4	7.9	11.2	…	…
Isotope Abundance Ge	…	…	…	…	…		…	…	20.5	
Collector Configuration M70	^{66}Zn	^{67}Zn	^{68}Zn	$^{137}Ba^{2+}$	…	^{70}Zn	…	…	^{72}Ge	^{73}Ge
Isotope Abundance Zn	27.7	4.0	18.5	…	…	0.6	…	…	…	…
Isotope Abundance Ge	…	…	…	…	…	20.5	…	…	27.5	7.8
Isotope Abundance Ba^{2+} ions	0.1	2.4	7.9	11.2	…	…	…	…	…	…

Note. All values are shown as percentages.

Table 5
Relative Mass Fractions of Major and Selected Trace Elements Released in the Seven Leaching Steps of the Four Carbonaceous Chondrites

Step	1	2	3	4	5	6	7	1	2	3	4	5	6	7
				Allende							Kainsaz			
Na	72	23	3	1	1	0	0	65	22	5	1	1	1	6
Mg	28	59	8	3	0	0	2	25	50	6	12	0	0	7
Al	10	44	15	3	2	0	26	17	59	10	1	1	0	11
P	14	79	5	2	0	0	0	21	73	5	2	0	0	0
S	5	54	21	<3	<3	19	<3	7	28	24	<3	<3	42	<3
K	61	35	3	<1	<1	<1	<1	78	22	<1	<1	<1	<1	<1
Ca	8	21	20	39	1	0	10	8	31	24	13	1	0	23
Ti	1	12	35	51	1	0	0	3	14	23	57	1	0	1
Cr	0	4	8	70	9	3	5	1	4	7	59	18	5	7
Mn	32	51	6	12	0	0	0	35	26	7	32	1	0	0
Fe	30	60	6	4	0	0	0	52	39	7	2	0	0	0
Ni	20	74	5	0	0	0	0	56	41	3	0	0	0	0
Cu	0	93	6	0	0	0	0	0	96	3	0	0	0	0
Zn	2	8	7	81	2	0	0	2	6	6	78	6	1	1
				Murchison							Colony			
Na	89	9	1	0	0	0	1	12	39	14	4	5	3	24
Mg	25	58	4	4	0	0	8	9	62	11	9	0	0	10
Al	29	58	4	0	1	0	8	5	62	26	1	1	0	6
P	22	74	3	1	0	0	0	5	34	59	2	0	0	0
S	21	32	11	<2	<2	36	<2	<11	39	61	<11	<11	<11	<11
K	71	27	<1	<1	<1	1	1	59	32	4	3	1	0	1
Ca	42	23	11	14	1	1	9	12	22	19	19	1	0	26
Ti	2	27	24	44	1	0	0	0	13	27	57	2	0	0
Cr	18	39	5	20	5	2	11	2	13	18	43	11	5	9
Mn	43	34	5	16	1	0	1	18	35	14	32	1	0	0
Fe	51	46	3	0	0	0	0	11	33	55	1	0	0	0
Ni	29	70	2	0	0	0	0	17	40	43	0	0	0	0
Cu	0	96	3	0	0	0	0	0	57	41	1	0	0	0
Zn	61	37	1	0	0	*<1	1	5	17	26	41	6	2	2

Note. Values are reported as percentages of the elements released in each step relative to the bulk elemental content.

for Allende and Kainsaz (3%–7%). Step 3 also accounts for most of the S in Colony (61%), while S in Step 6 was below detection limit, in contrast to the substantial S fractions released in Step 6 for Allende and Kainsaz (19%–42%). Furthermore, a large fraction of Zn is leached earlier (17% in Step 2 and 26% in Step 3), and a much larger fraction of Na was released later (24% in Step 7) compared to Allende (0%) or Kainsaz (6%). Nonetheless, Steps 4 and 5 for Colony display similar compositions to Allende and Kainsaz, including mainly Ca, Ti, Cr, and Zn.

Finally, Murchison displays some distinct leachate patterns compared to the other meteorites. Most elements were still leached primarily in Steps 1 and 2 (53%–98%); however, unlike in the other meteorites, most of the Zn was also leached in the first two steps (98%). As for Allende and Kainsaz, a substantial fraction of S was released in Step 6 (36%). Lastly, noticeable amounts of Ca, Ti, Cr, and Mn are present in Steps 3–5, but primarily in Step 4 (14%–44%), such that, apart from the low Zn content, these steps are comparable to the other meteorites.

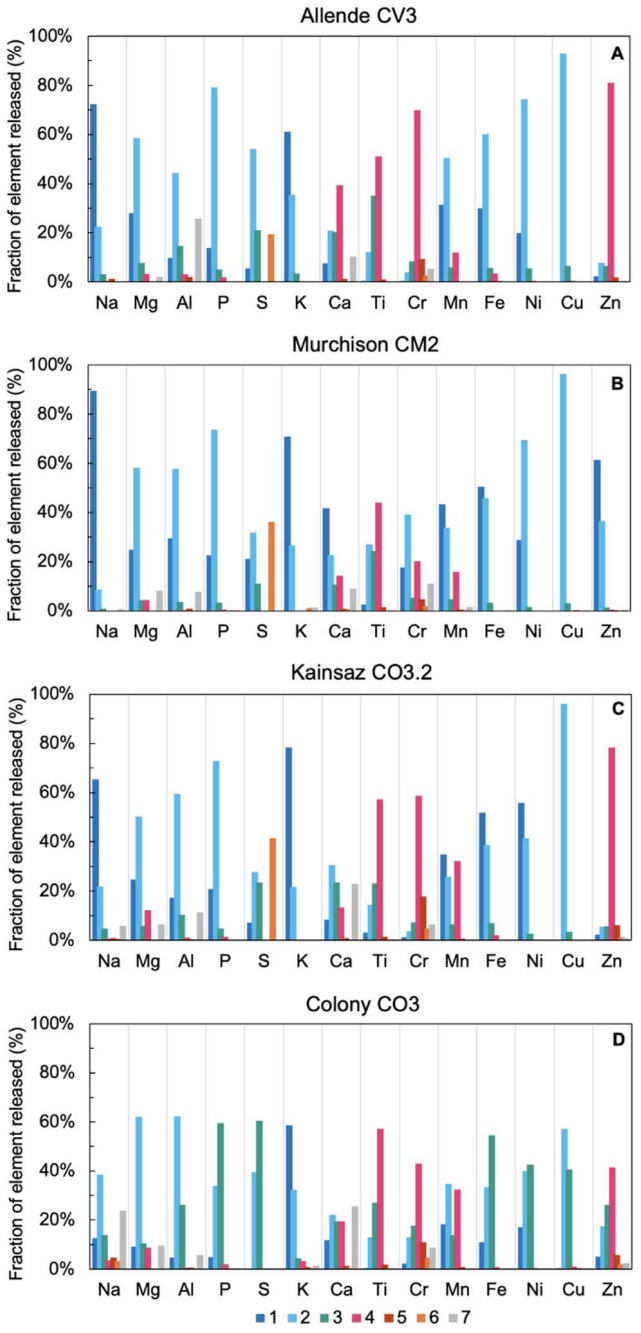


Figure 2. Major and some selected trace element results from elemental analyseis for leachates of (A) Allende CV3, (B) Murchison CM2, (C) Kainsaz CO3.2, and (D) Colony CO3. Steps: (1) Acetic Acidacid; (2) HNO3; (3) HCl; (4) HCl–HF 100°C; (5) HCl–HF 160°C; (6) HNO3–HF 160°C; (7) HNO3–HF 180°C. Results are available in Table 5.

3.2. Mass-independent Zn Isotope Analyses

The Zn isotope compositions of the leachates, as well as the Zn fractions, are shown in Tables 6 and 5 and in Figures 3–5 and 2, respectively. Results that employ the $^{66}Zn/^{67}Zn$ normalization are primarily adopted in the discussion, unless otherwise noted. The notation $\varepsilon^{i}Zn$ is hence used for this normalization, while an $\varepsilon^{i}Zn_{67/64}$ notation is employed for results obtained with internal normalization to $^{64}Zn/^{67}Zn$. Furthermore, because $\varepsilon^{64}Zn$ is best resolved between samples, it is highlighted in Figure 4. With few exceptions, the samples showcase enrichments in the NR Zn isotopes, which translates to negative $\varepsilon^{64}Zn$, and positive $\varepsilon^{68}Zn$ and $\varepsilon^{70}Zn$ values, a pattern that is characteristic of bulk CCs (R. Martins et al. 2023). However, a few leaching steps are identical to the London Zn standard within uncertainties, while others show complementary εZn patterns that are characteristic of NC rather than CC meteorites.

In detail, Steps 1, 2, 3, 4, 5, and 7 for Allende all show isotope compositions that are identical to the bulk values, as reported in R. Martins et al. (2023) and in Table 6. However, Step 6 shows a resolvable depletion in ^{68}Zn ($\varepsilon^{68}Zn_{Allende(6)} = -0.33 \pm 0.20$), as would be expected for an NC meteorite. Step 6 for Murchison shows similar features, with a resolvable enrichment in ^{64}Zn compared to the London Zn standard ($\varepsilon^{64}Zn_{Murchison(6)} = 0.61 \pm 0.42$). Conversely, Steps 1, 2, 3, 4, and 7 of Murchison are identical to the bulk within uncertainties. Step 5 is the only step that is enriched in NR isotopes relative to bulk Murchison ($\varepsilon^{64}Zn_{Murchison(5)} = -2.29 \pm 0.31$).

Colony displays very similar results for most leachates, and these overlap with the bulk value of MIL 090025, the only CO chondrite for which results employing the same ratio for internal normalization were available from previous work (R. Martins et al. 2023). The sole exception is Step 1, which is unresolvable from London Zn. Finally, most steps for Kainsaz also largely overlap with and are indistinguishable from the bulk values for MIL 090025. However, some isotope ratios for Steps 1, 6, and 7 are also identical to the London Zn standard within error.

A bulk nucleosynthetic Zn isotope composition was calculated for each meteorite based on the compositions of the leaching steps and their respective Zn fractions as follows:

$$\varepsilon^{i}Zn_{bulk} = \sum_{n=1}^{7} \varepsilon^{i}Zn_{n} \times f_{Zn}^{n} \quad (2)$$

where i is the isotope of interest, n corresponds to the leaching step, and f_{Zn}^{n} is the fraction of Zn for step n. The uncertainties were calculated using the following equation:

$$2SD_{bulk}^{i} = \sqrt{\sum_{n=1}^{7} (f_{Zn}^{n} \times 2SD_{n}^{i})^{2}} \quad (3)$$

where $2SD_{n}^{i}$ is the standard error of the mean of all repeats performed for each leaching step. Table 6 compares the calculated $\varepsilon^{i}Zn$ values and respective uncertainties for the bulk meteorites with previously measured bulk values for Allende, Murchison, and MIL 090025 (R. Martins et al. 2023, 2024).

Notably, P. S. Savage et al. (2022) also performed sequential leaching on an aliquot of Murchison. Since (1) the adopted leaching procedures were different, and (2) some of the steps in P. S. Savage et al. (2022) did not yield enough Zn to allow for isotope measurements, a direct comparison between the results is not possible. The $\varepsilon^{68}Zn_{67/64}$ values reported by P. S. Savage et al. (2022) show resolvable anomalies for their steps 1, 3, and 4, while the remaining steps are indistinguishable from the terrestrial standard. However, the bulk $\varepsilon^{68}Zn_{67/64}$ value determined for Murchison in that study also overlaps with the terrestrial standard, making it difficult to make any assertions based on these results. In contrast, the $\varepsilon^{66}Zn_{67/64}$ values reported by P. S. Savage et al. (2022) for Murchison leachates differ from the terrestrial composition for all steps and for the bulk sample ($\varepsilon^{66}Zn_{67/64} = 0.16 \pm 0.06$ to 0.47 ± 0.06). The steps that

Table 6
Mass-independent Zn Isotope Data (in ε^{i}Zn notation) for the Seven Leachate Fractions of the Four Meteorites, as Well as Bulk Composition of the Terrestrial Rock Standard BCR-2, and Calculated and Measured Bulk Compositions of the Meteorites

Sample	Leaching Step	Data Normalized to $^{66}Zn/^{67}Zn$						Data Normalized to $^{64}Zn/^{67}Zn$			
		$\varepsilon^{64}Zn$	n	$\varepsilon^{68}Zn$	n	$\varepsilon^{70}Zn$	n	$\varepsilon^{66}Zn_{67/64}$	n	$\varepsilon^{68}Zn_{67/64}$	n
Allende CV3	1	−1.00 ± 0.67	2	0.41 ± 0.26	2	…	…	0.31 ± 0.22	2	0.08 ± 0.11	2
	2	−0.82 ± 0.63	2	0.24 ± 0.21	2	…	…	0.36 ± 0.21	2	0.11 ± 0.21	2
	3	−0.63 ± 0.29	4	0.16 ± 0.11	4	…	…	0.19 ± 0.19	3	−0.07 ± 0.13	3
	4	−1.13 ± 0.22	9	0.42 ± 0.09	14	1.57 ± 0.57	9	0.43 ± 0.05	9	0.12 ± 0.06	9
	5	−1.10 ± 0.18	11	0.35 ± 0.10	16	1.14 ± 0.23	9	0.38 ± 0.06	11	−0.02 ± 0.13	11
	6	0.03 ± 0.59	2	−0.33 ± 0.20	2	…	…	−0.03 ± 0.19	2	−0.33 ± 0.14	2
	7	−0.99 ± 0.74	1	0.41 ± 0.24	1	…	…	0.33 ± 0.24	1	0.12 ± 0.18	1
Calculated Bulk	…	−1.07 ± 0.19	…	0.39 ± 0.08	…	…	…	0.38 ± 0.06	…	0.05 ± 0.10	…
Measured Bulk	…	−0.91 ± 0.21	…	0.36 ± 0.15	…	…	…	0.30 ± 0.07	…	0.13 ± 0.11	…
Murchison CM2	1	−0.88 ± 0.13	4	0.36 ± 0.09	9	0.67 ± 0.49	5	0.29 ± 0.04	4	0.12 ± 0.11	4
	2	−0.64 ± 0.17	6	0.43 ± 0.11	8	0.81 ± 0.45	2	0.21 ± 0.06	6	0.20 ± 0.29	6
	3	−0.46 ± 0.58	2	0.15 ± 0.43	5	0.00 ± 0.60	3	0.15 ± 0.21	2	−0.11 ± 0.37	2
	4	−1.40 ± 0.42	2	0.36 ± 0.23	4	0.43 ± 0.60	2	0.46 ± 0.14	2	0.07 ± 0.20	2
	5	−2.29 ± 0.31	2	0.50 ± 0.21	2	2.31 ± 0.46	2	0.86 ± 0.20	2	−0. 22 ± 0.27	2
	6	0.61 ± 0.42	1	−0.34 ± 0.37	1	…	…	−0.10 ± 0.27	2	−0.25 ± 0.29	2
	7	−0.62 ± 0.50	1	0.46 ± 0.37	1	1.31 ± 0.46	1	0.24 ± 0.16	1	0.20 ± 0.22	1
Calculated Bulk	…	−0.79 ± 0.10	…	0.38 ± 0.08	…	…	…	0.26 ± 0.03	…	0.15 ± 0.13	…
Measured Bulk	…	−1.32 ± 0.34	…	0.53 ± 0.09	…	…	…	0.28 ± 0.03	…	0.29 ± 0.07	…
Colony CO3	1	0.16 ± 0.38	5	−0.10 ± 0.11	7	0.37 ± 0.68	2	−0.05 ± 0.13	5	−0.14 ± 0.12	5
	2	−0.78 ± 0.26	4	0.38 ± 0.12	10	1.18 ± 0.25	6	0.26 ± 0.08	4	0.08 ± 0.09	4
	3	−0.63 ± 0.07	4	0.32 ± 0.14	8	0.76 ± 0.25	4	0.21 ± 0.02	4	0.03 ± 0.18	4
	4	−1.05 ± 0.45	3	0.37 ± 0.17	7	0.76 ± 0.21	4	0.35 ± 0.15	3	0.17 ± 0.20	3
	5	−0.69 ± 0.25	9	0.30 ± 0.12	12	0.81 ± 0.41	3	0.23 ± 0.08	9	0.02 ± 0.09	9
	6	−0.70 ± 0.23	5	0.18 ± 0.21	8	0.29 ± 0.70	3	0.23 ± 0.08	5	−0.11 ± 0.28	5
	7	−0.83 ± 0.24	4	0.13 ± 0.21	7	0.38 ± 0.65	3	0.27 ± 0.08	4	−0.15 ± 0.40	4
Calculated Bulk	…	−0.79 ± 0.19	…	0.32 ± 0.08	…	0.80 ± 0.13	…	0.38 ± 0.03	…	0.11 ± 0.09	…
Measured Bulk	…	−0.57 ± 0.22	…	0.16 ± 0.14	…	0.78 ± 0.25	…	0.19 ± 0.07	…	−0.08 ± 0.15	…
Kainsaz CO3.2	1	−0.38 ± 0.14	11	0.09 ± 0.08	11	0.51 ± 0.35	6	0.16 ± 0.05	11	−0.01 ± 0.07	11
	2	−0.76 ± 0.10	11	0.20 ± 0.16	16	1.45 ± 0.16	16	0.26 ± 0.03	11	0.02 ± 0.16	11
	3	−0.66 ± 0.23	11	0.29 ± 0.15	11	1.23 ± 0.33	6	0.21 ± 0.09	11	0.10 ± 0.11	11
	4	−0.65 ± 0.23	12	0.17 ± 0.16	12	1.30 ± 0.49	5	0.21 ± 0.08	12	−0.05 ± 0.12	12
	5	−0.90 ± 0.17	11	0.29 ± 0.15	16	1.03 ± 0.28	11	0.29 ± 0.08	11	−0.06 ± 0.16	11
	6	−0.32 ± 0.60	3	−0.01 ± 0.26	5	0.26 ± 0.54	2	0.13 ± 0.28	3	−0.19 ± 0.13	3
	7	−0.13 ± 0.67	2	0.17 ± 0.24	5	1.37 ± 0.27	4	0.06 ± 0.22	2	−0.24 ± 0.14	2
Calculated Bulk	…	−0.66 ± 0.18	…	0.18 ± 0.44	…	1.26 ± 0.85	…	0.21 ± 0.07	…	−0.04 ± 0.10	…
Measured Bulk	…	−0.57 ± 0.44	…	0.16 ± 0.14	…	0.78 ± 0.25	…	0.19 ± 0.07	…	−0.08 ± 0.15	…
BCR-2	…	−0.04 ± 0.11	22	0.07 ± 0.06	42	0.00 ± 0.12	33	0.01 ± 0.04	22	0.05 ± 0.07	22

Note. n: total number of individual analytical runs for a given sample. Calculated bulk values are based on the mass-independent Zn isotope compositions and Zn mass fractions determined for the leaching steps of each meteorite. Measured values determined for the bulk samples are from R. Martins et al. (2023) and R. Martins et al. (2024). No measured bulk data obtained using $^{66}Zn/^{67}Zn$ for internal normalization are available for Colony and Kainsaz; the composition of MIL 090025 CO3 is hence shown for comparison.

attack more labile phases (steps 1–4) leached most of the Zn and are bulk-like, similar to the results presented in this study (Steps 1–2). Nevertheless, our results show that the minerals attacked in Step 5 display the most extreme composition ($\varepsilon^{66}Zn_{64/67\text{-Murchison(5)}} = 0.86 \pm 0.20$), which is not observed for any of the steps reported by P. S. Savage et al. (2022). It is, however, possible that the minerals attacked in Step 5 of this study, which released just ~0.4% of the total Zn, were attacked by Steps 6 and/or 7 in the procedure adopted by P. S. Savage et al. (2022), which did not yield enough Zn for isotopic measurements to be performed. In both studies, these are among the first steps to involve HF and HCl at high molarities and/or temperatures, and both yielded low Zn fractions. Likewise, the NC-like Zn released in Step 6 of this study ($\varepsilon^{66}Zn_{64/67\text{-Murchison(6)}} = -0.10 \pm 0.27$) was possibly targeted by Step 9 of P. S. Savage et al. (2022), which was not measured due to the low Zn content. Both of these steps involve the use of high molarity acids and high temperatures and are expected to attack more acid-resistant phases.

4. Discussion

4.1. Constraints from Leachate Compositions on Zn-bearing Phases in Carbonaceous Chondrites

Zinc is variably distributed between the seven leaching steps of the four meteorites characterized in this study. Using acetic acid, most of the Zn in Murchison was leached in Step 1 (61%), along with most of the Na, and K, and considerable fractions of Al, Mg, P, S, Ca, Mn, Fe, and Ni (Figure 2, Table 5). The large Na, K, and Zn fractions in this step most likely result from mobilization induced by the extensive aqueous alteration that took place in the CM parent bodies (A. Rubin et al. 2007; A. J. King et al. 2017). This process hence transferred these aqueously mobile elements to

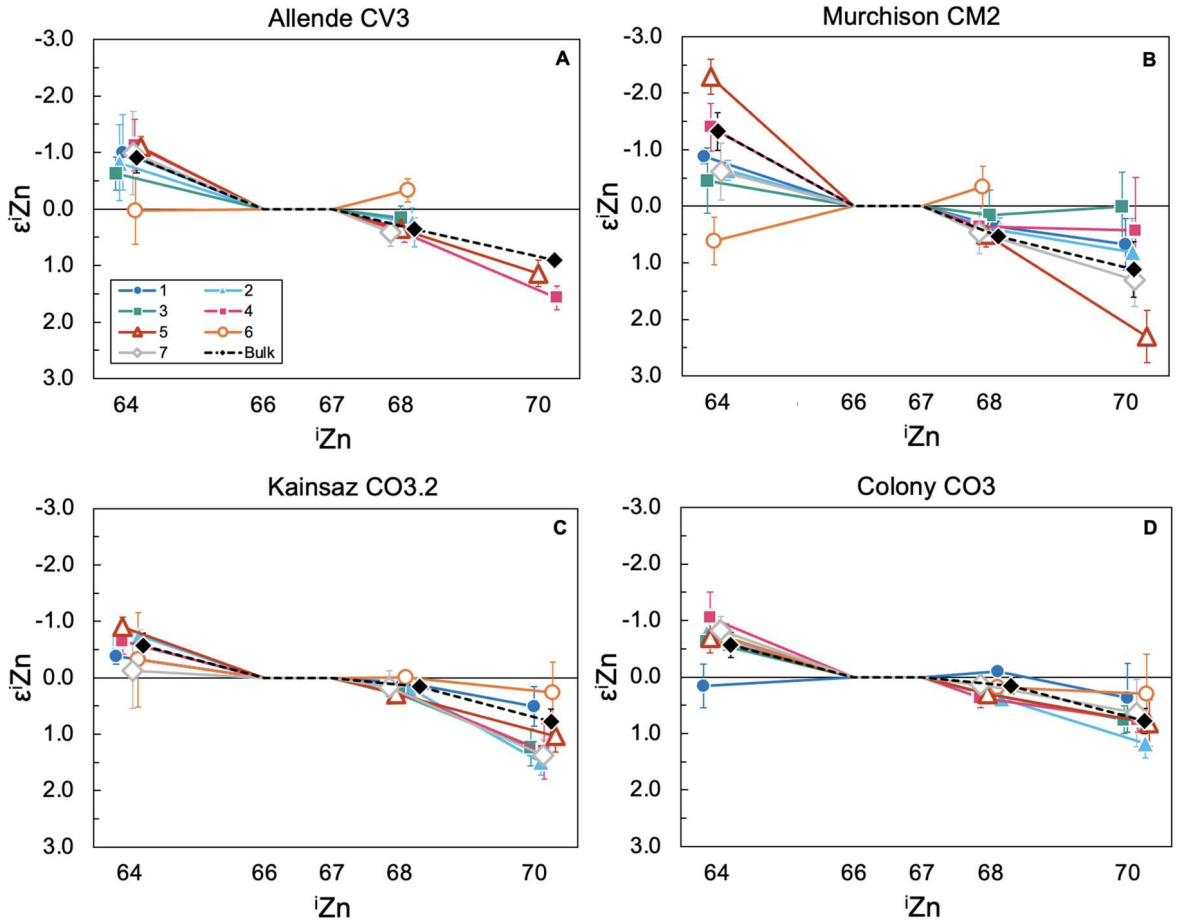


Figure 3. Mass-independent Zn isotope compositions in ε^{i}Zn notation. Results for the leaching steps of (A) Allende CV3, (B) Murchison CM2, (C) Kainsaz CO3.2, and (D) Colony CO3 (Table 5). Measured bulk compositions of Allende CV3, Murchison CM2, and MIL 0922025 CO3 (R. Martins et al. 2023, 2024) are plotted for comparison. As an excess of anomalous neutron-rich (NR) Zn results in negative ε^{64}Zn values, the *y*-axes are flipped so that the more NR samples (with more negative ε^{64}Zn values) are clearly highlighted as more anomalous.

secondary, more labile phases, such as carbonates, phosphates, and phyllosilicates. Iron and Mg released in this step may be derived from the leaching of very fine-grained matrix material. This likely includes glass from the mesostasis, serpentine, tochilinite-cronstedtite intergrowths, and potentially olivine and pyroxene present in CMs (A. Rubin & C. Ma 2021a, 2021b; A. N. Krot et al. 2014), in addition to carbonates, which also carry Ca, Fe, and Mn. A minor fraction of sulfides and some of the rare metals may also have been leached in this step. Kainsaz and Allende leachates have roughly similar elemental compositions as Murchison for Step 1, apart from the much lower Zn content (2%), which may reflect the more limited aqueous alteration history of these chondrites such that Zn is not hosted in easily soluble phases. For these meteorites, Step 1 likely attacked grain surfaces and very small grains, possibly including fine-grained matrix minerals, sulfides, Fe–Ni metal, and amorphous silicates, which are major phases in COs and CVs (A. Rubin & C. Ma 2021a, 2021b; A. N. Krot et al. 2014). The composition of Step 1 for Colony is also similar, but the mass fractions that were released are more limited compared to the other meteorites, which possibly relates to the effects of terrestrial weathering.

The Zn contents increase by a factor of 3–4 from Step 1 (acetic acid) to Step 2 (HNO_3) for Allende (8%), Kainsaz (6%), and Colony (15%), while almost all of the remaining Zn is released in Step 2 for Murchison (37%). Again, these differences potentially result from the parent body alteration experienced by Murchison, which may have caused redistribution of Zn. Combined, the first two steps account for most of the Fe, and Mg, as well as much of the Na, Al, Ca, and Mn. This suggests that the main silicate components of the matrix and chondrules (i.e., olivine and pyroxene) were largely attacked in these first steps. Step 2 also contains large fractions of P, S, Fe, and Ni, and most of the Cu (54%–96%). As such, this step likely targeted most of the metal, sulfides, sulfates, and phosphates present in these meteorites.

Step 3 (HCl) contains limited Zn fractions (1%–7%) for all meteorites, except for Colony (26%). Steps 1 and 2 for Colony released a larger fraction of Zn than for Kainsaz and Allende, possibly due to the conditioning effects of terrestrial weathering on the mineralogical composition. A general observation is that Step 3 has an intermediate composition between Steps 2 and 4, as it appears to have leached most of the remaining metal, sulfide, and phosphate phases (P, S, Fe, Ni, Cu), as well as variable fractions of the elements that were leached primarily in Step 4.

Step 4 (HCl–HF) is the first step to employ HF, and its composition is distinct from previous steps. This step released the largest Zn fractions for all meteorites (41%–81%) except for Murchison (0.3%), along with large amounts of Ti (46%–60%), and Cr (21%–73%), substantial fractions of Ca (14%–

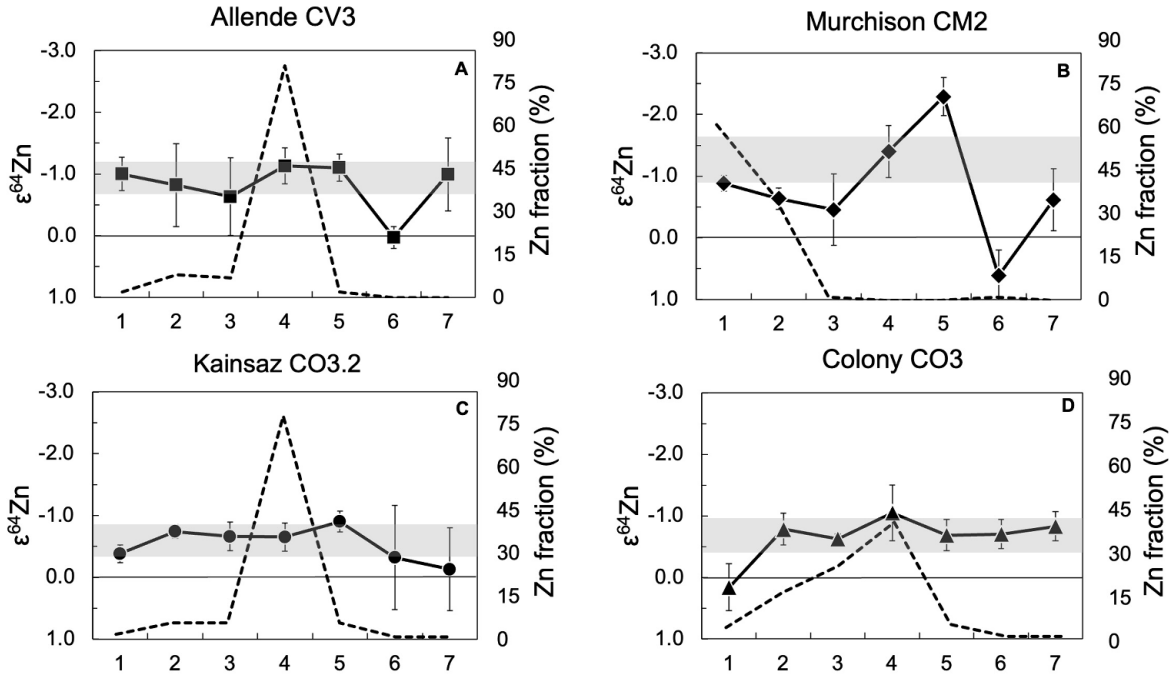


Figure 4. ε^{64}Zn (data points and solid line) and percentage of Zn mass fraction (stippled line) for the leaching Steps 1–7 of (A) Allende CV3, (B) Murchison CM2, (C) Kainsaz CO3.2, and (D) Colony CO3 (Table 6). For comparison, the gray bands show the measured mean ε^{64}Zn and uncertainties determined for Allende CV3, Murchison CM2, and MIL 0922025 CO3 (R. Martins et al. 2023, 2024; Table 6) for comparison. As an excess of anomalous NR Zn results in negative ε^{64}Zn values, the y-axes are flipped so that the more NR samples (with more negative ε^{64}Zn values) are clearly highlighted as more anomalous.

44%) and Mn (14%–35%), a small Mg fraction (4%–13%) and only very limited Fe and Al. Step 5 (also HCl–HF) contains the same elements, but with much more limited mass fractions. As such, even though the Zn fractions released in this step are small (up to 6%), they provide the second-largest elemental fractions after Cr (up to 18%). As this step applied the same acid mixture as Step 4, but at higher temperatures, it likely targeted similar phases that were not completely digested in the previous step.

As the first steps to employ HF, it would be expected that Steps 4 and 5 would leach silicates (M. Rotaru et al. 1992). However, the distribution of Fe and Mg among the leachates suggest that most of the major ferromagnesian silicate minerals of these meteorites (olivine, pyroxene, and phyllosilicates) were primarily leached in Steps 1 and 2. The remaining Fe and Mg leached in Steps 4 and 5 may therefore have been leached from more acid-resistant/larger silicate grains. Nonetheless, the small fractions of Fe (0.2%–6%), Mg (4%–13%), and Al (1%–6%), combined with the substantial amounts of Ca, Ti, Mn, Cr, and Zn, in these steps are compatible with leaching of some oxide minerals. They may include magnetite, ilmenite, or hibonite, which are less abundant than the main carriers of Fe, Mg, and Al leached in Steps 1–3, but could account for substantial fractions of Ti and Ca. The large Cr fractions in Steps 4 and 5 may furthermore be linked to leaching of chromite or Cr-spinels, which can also be enriched in Zn in some meteorites (J.-M. Luck et al. 2005; L. J. Bridgestock et al. 2014). These oxides are present in all CC groups analyzed in this study, either as primary phases or alteration minerals in matrix (i.e., magnetite), chondrules (i.e., chromite), and refractory components (i.e., hibonite, spinel; A. Rubin & C. Ma 2021a, 2021b; A. N. Krot et al. 2014). Hence, the main Zn carriers in Allende, Kainsaz, and Colony are possibly acid-resistant silicates and/or oxides.

Step 6 (HNO_3–HF) dissolved relatively minor elemental fractions, including for Zn (up to 2%), but it released a considerable amount of S for Allende, Murchison, and Kainsaz (22%–43%), suggesting the presence of some acid-resistant sulfides/sulfates (P. Robinson 2025). The only exception is Colony, for which S was below detection limit. This could be a result of terrestrial alteration that caused loss of this acid-resistant S-bearing phase in Colony. Finally, Step 7 (several treatments with HNO_3, HF, and HCl including pressure digestion) contains minor Zn fractions (up to 2%) and is dominated by Na, Mg, Al, Ca, and Cr. This step likely targeted more refractory, acid-resistant grains of oxides (chromite, ilmenite, melilite, spinel, hibonite, perovskite, and corundum), carbides (SiC), diamond, and graphite, which can be present either as part of refractory components (CAIs) or as presolar grains (A. Rubin & C. Ma 2021a, 2021b; G. R. Huss et al. 2003). Some of the Ca and Al may also reflect the redissolution of secondary fluorides that precipitated during the previous HF-bearing leaching steps.

4.2. Re-equilibration and Homogenization of Zn Isotope Compositions

From the steps that attack more labile and/or fine-grained phases (Steps 1–2; silicates, sulfates, sulfides, carbonates, phosphates, metal, and phyllosilicates), to those that digest more acid-resistant and potentially larger mineral grains (silicates, oxides, and refractory minerals; Steps 3–7), every step shows evidence for the presence of anomalous, i.e., nonterrestrial Zn in at least one of the meteorites. In most cases, the anomalies correspond to an excess of the NR isotopes, equivalent to negative ε^{64}Zn, and positive ε^{68}Zn and ε^{70}Zn values (Figures 3–5). This is not surprising, as the bulk CC compositions display this pattern (P. S. Savage et al. 2022; T. Steller et al. 2022; R. Martins et al. 2023). However, an

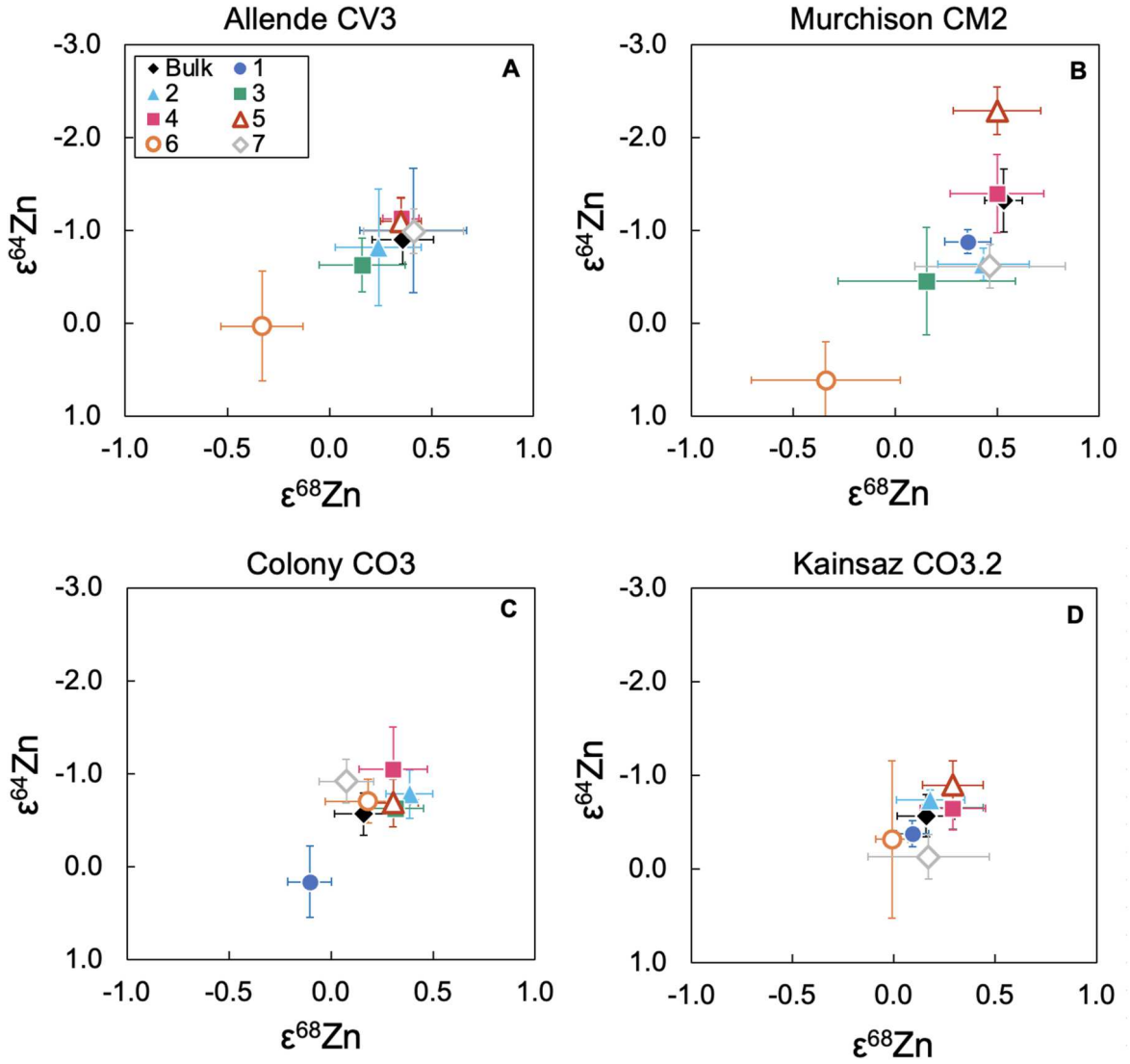


Figure 5. Mass-independent Zn isotope compositions in ε^{i}Zn notation. Results for the leaching steps of (A) Allende CV3, (B) Murchison CM2, (C) Kainsaz CO3.2, and (D) Colony CO3 (Table 6). As an excess of anomalous NR Zn results in negative ε^{64}Zn values, the *y*-axes are flipped so that the more NR samples (with more negative ε^{64}Zn values) are clearly highlighted as more anomalous.

opposite, nonterrestrial NC-like trend is revealed by the clearly resolved positive ε^{64}Zn value for Step 6 of Murchison ($\varepsilon^{64}Zn_{Murchison(6)} = 0.61 \pm 0.42$), and a negative ε^{68}Zn value for Allende ($\varepsilon^{68}Zn_{Allende(6)} = -0.33 \pm 0.20$).

Some leachates hence display resolvable differences from each other, defining a limited, but clear range in isotope compositions ($\varepsilon^{64}Zn_{Murchison(5)} = -2.29 \pm 0.31$ to $\varepsilon^{64}Zn_{Murchison(6)} = 0.61 \pm 0.42$). This stands in contrast to what is observed for refractory elements, which typically exhibit larger isotope anomalies relative to the bulk composition in some of the leaching steps, establishing a much wider range in compositions (e.g., A. Trinquier et al. 2009; C. Burkhardt & M. Schönbächler 2015). An example of this is nucleosynthetic Ti isotope variations in leachates of the CI meteorite, Orgueil, for which some steps display significant deviations from bulk values and cover a range that far exceeds the variations observed for bulk CCs ($\varepsilon^{50}Ti_{Orgueil\text{-}3b} = -0.48 \pm 0.04$ to $\varepsilon^{50}Ti_{Orgueil\text{-}4} = 10.38 \pm 0.28$, compared to $\varepsilon^{50}Ti_{Orgueil\text{-}bulk} = 1.87 \pm 0.04$; A. Trinquier et al. 2009). This suggests that the anomalous Ti was hosted by minerals that were targeted primarily in the most anomalous steps. Such extreme deviations from the bulk isotope values are not evident for Zn, even though the anomalous Zn is thought to be produced by the same nucleosynthetic process that generated the variable ε^{50}Ti values observed in meteorites (R. Martins et al. 2023, 2024).

The much more limited variations in nucleosynthetic Zn isotope compositions between leaching steps may reflect the volatile character of Zn. In line with this, nucleosynthetic Pd isotope variations of bulk meteorites are smaller than anomalies observed for more refractory elements with similar atomic masses, such as Mo and Ru (M. Ek et al. 2020). This was suggested to reflect less efficient condensation of Pd into presolar grains around asymptotic giant branch stars, due to its lower condensation temperature (M. Ek et al. 2020). Accordingly, it is possible that the less-expressive Zn isotope variations recorded by the leachates reflect that Zn condensed much less efficiently into its respective presolar carriers than more refractory elements from the same stellar sources, such as Ca and Ti.

Alternatively, it is also plausible that the compositions of different mineral phases were altered during equilibration

within the parent body or through destruction of presolar host grains. If so, more extreme isotope variations were possibly present initially, but these were more efficiently homogenized for Zn than for refractory elements. Multiple leaching steps that presumably targeted distinct mineral phases exhibit similarly anomalous Zn isotope compositions (Figures 3–5), ranging from the steps that likely target alteration products such as phyllosilicates ($\varepsilon^{68}Zn_{Allende(1)} = 0.41 \pm 0.26$), to the refractory oxide grains inferred to have been leached in Step 7 ($\varepsilon^{68}Zn_{Allende(7)} = 0.41 \pm 0.24$). However, it is unlikely that the stellar sources that generated the anomalous Zn would have produced such a mineralogically diverse set of presolar grains. Hence, the presence of bulk-like Zn in all leaching steps may not be an original feature. Instead, the anomalous Zn is probably no longer hosted solely in its original carrier phase, but rather, it was redistributed into one or several secondary phases.

C. Burkhardt & M. Schönbächler (2015) showed that the nucleosynthetic W isotope compositions of leachates from different CC meteorites are progressively more homogeneous for parent bodies that record higher levels of thermal alteration. This is particularly evident for their Step 5 of the thermally pristine CI chondrite Orgueil, which is very distinct from the bulk composition ($\varepsilon^{183}W_{O5} = -40.52 \pm 1.79$ compared to $\varepsilon^{183}W_{O_bulk} = -0.23 \pm 0.84$ for the bulk). This contrast is much less prominent for Murchison ($\varepsilon^{183}W_{M5} = -19.17 \pm 0.86$ compared to $\varepsilon^{183}W_{M_bulk} = -0.30 \pm 0.60$), and completely absent for Allende, which records substantial thermal metamorphism ($\varepsilon^{183}W_{A5} = -1.77 \pm 2.00$ compared to $\varepsilon^{183}W_{A_bulk} = -0.12 \pm 0.56$). Since it is significantly more volatile, Zn likely records even larger extents of homogenization through thermal alteration within the parent bodies than W. This is consistent with our results, which show that the leaching steps in the COs and Allende CV3 have mostly bulk-like Zn isotope compositions (Figures 3–5), while the less thermally altered Murchison displays more variable compositions between the different steps, ranging from $\varepsilon^{64}Zn_{(5)} = -2.29 \pm 0.31$ to $\varepsilon^{64}Zn_{(6)} = 0.61 \pm 0.42$.

Yet another possibility is that the different extents of nucleosynthetic isotope variations determined for leachates of distinct meteorites reflect variable abundance of matrix. In detail, while CIs are composed almost entirely of matrix, only ~70% of the Murchison volume corresponds to matrix, and COs and CVs contain just 30%–40% (Krot et al. 2005). Therefore, COs and CVs contain substantially more reprocessed material in the form of chondrules, and refractory inclusions, such that the isotope compositions were more extensively homogenized during the formation of these high-temperature components. Despite of pervasive aqueous alteration, CM chondrites like Murchison still preserve more presolar grains simply because more were initially present due to the higher matrix content (G. R. Huss et al. 2003), and this is now reflected in the more variable Zn isotope compositions of the leachates.

In any case, it is likely that the Zn isotope compositions of the phases attacked by the different leaching steps of this study were variably homogenized either in the interstellar medium (ISM), within the parent bodies, during high-temperature processing in the protoplanetary disk, or a combination thereof. Consequently, the current Zn isotope compositions of the phases are more homogeneous and similar to the bulk values than in their initial state. If so, then more extreme compositions are likely recorded by the less thermally altered matrix of chondrule-free CI chondrites.

4.3. Carrier Phases of Isotopically Anomalous Zn

The small but resolvable Zn isotope differences between some leachate steps reveal that the various mineral phases were not fully homogenized, and, as such, some inferences can be made about the original distribution of the anomalous Zn. For example, Step 1 is identical to the bulk composition for all meteorites except Colony, where it is indistinguishable from the London Zn standard. Since Colony is the only meteorite find, this most likely reflects terrestrial contamination. Overall, it is to be expected that Step 1 targeted many of the alteration minerals in all meteorites, and these would have contained Zn that was originally present in other phases. This can likely be extended to Steps 2 and 3, which also digested more labile phases with mostly bulk-like εZn values.

Step 4 displays bulk-like isotope compositions, and it released the largest fraction of Zn for all meteorites except Murchison. The most anomalous composition is observed for Step 5 of Murchison, which clearly differs from the bulk values ($\varepsilon^{64}Zn_{Murchison(5)} = -2.29 \pm 0.31$; Figures 3–5). These two steps employed an HCl–HF mixture at high temperatures (Table 2), and released primarily Ti, Zn, and Cr, and substantial Ca and Mn, such that they likely targeted oxides and/or acid-resistant silicates. It is hence likely that the NR Zn was originally concentrated in these phases.

A previous leaching experiment performed on Orgueil (A. Trinquier et al. 2009) revealed that isotopically anomalous Ti was primarily released in a leaching step that employed 3 M HCl–14 M HF for 4 days at 100°C, and which is hence similar to Step 4 of this study. Modeled nucleosynthetic isotope anomalies that were obtained using predicted yields of SN Ia (S. E. Woosley 1997) and electron capture core collapse supernovae (ECSNe; S. Wanajo et al. 2013) suggest that the anomalous NR Zn is likely derived from the same nucleosynthetic source that also produced excesses of ^{48}Ca and ^{50}Ti (N. Dauphas et al. 2014; R. Martins et al. 2023, 2024). Furthermore, the carrier phase(s) of the anomalous Ca and Ti were hypothesized to be oxides, and in particular perovskite (N. Dauphas et al. 2014). As such, the isotopically anomalous Ca, Ti, and Zn could be hosted in similar presolar carriers—possibly oxides—derived from the same stellar sources.

Notably, the magnitude of Zn isotope anomalies in CCs is smaller than expected for their given ^{50}Ti enrichments (R. Martins et al. 2023, 2024). However, this decoupling is likely due to the addition and variable abundance of CAIs in CCs. These refractory components host substantial amounts of Ti with very significant ^{50}Ti enrichments (e.g., Z. A. Torrano et al. 2019). Previous studies have shown that mixing between a CI-like and a CAI-like component can account for some of the nucleosynthetic Ti isotope variability observed for bulk CCs (A. Trinquier et al. 2009; H. Palme & K. Mezger 2024). However, due to their high condensation temperatures, CAIs initially contained very limited Zn, such that the variable presence of CAIs in different CCs has only a minimal impact on the mass-dependent Zn isotope compositions of the meteorites (J.-M. Luck et al. 2005). A similarly limited effect is therefore expected for the nucleosynthetic Zn isotope compositions of bulk CCs.

In contrast to Steps 4 and 5, Step 6 is depleted in NR isotopes compared to the bulk, with a small but resolvable

positive ε^{64}Zn value in Murchison ($\varepsilon^{64}Zn_{Murchison(6)} = 0.61 \pm 0.42$), and a negative ε^{68}Zn value for Allende ($\varepsilon^{68}Zn_{Allende(6)}$) = –0.33 ± 0.20; (Figures 3 and 5), akin to NC meteorites (R. Martins et al. 2023). This step is furthermore identical to the terrestrial London Zn standard for Kainsaz ($\varepsilon^{68}Zn_{Kainzas(6)} = –0.01 \pm 0.26$) and displays a bulk-like composition for Colony ($\varepsilon^{68}Zn_{Colony(6)} = -0.70 \pm 0.23$). Notably, Step 6 appears to have attacked acid-resistant sulfides/sulfates (Table 5, Figure 2). Such phases were apparently almost completely absent in Colony, which would explain the lack of any NC- or Earth-like isotope signatures for this meteorite. The similarities with the London Zn standard could reflect terrestrial contamination for Kainsaz. However, the resolvable depletions in NR isotopes relative to the terrestrial standard for Murchison and Allende cannot be attributed to terrestrial contamination. It therefore appears that Step 6 targeted phases that were originally depleted in NR isotopes, to an extent that occasionally exceeds the depletion of these isotopes in terrestrial samples.

Step 7 targets more acid-resistant phases, which likely include refractory minerals (M. Rotaru et al. 1992), encompassing both presolar grains such as SiC, spinels, diamonds, and graphite (K. Lodders & S. Amari 2005), as well as high-temperature condensates, such as the minerals that were incorporated by CAIs and amoeboid olivine aggregates. Due to their high condensation temperatures, it is unlikely that the refractory phases attacked in Step 7 incorporated substantial amounts of Zn during condensation of presolar grains near the stellar sources or during crystallization in the high-temperature environments in which CAIs formed. These phases potentially include Zn that was implanted by supernovae shockwaves in the ISM in the case of presolar grains (A. J. King et al. 2012), as well as by solid–gas interactions in the protoplanetary disk (J.-M. Luck et al. 2005). Indeed, the measured Zn mass fractions for Step 7 are limited, ranging from 0.4% for Allende to 2.3% for Colony, with the leachates displaying compositions that are indistinguishable from the bulk for all meteorites. As such, the most acid-resistant phases are also unlikely to be the original hosts of the NR Zn.

4.4. Testing the Thermal Processing Model

The observed heterogeneous distribution of isotopes produced by explosive nucleosynthesis in the solar system has been suggested to result from the destruction of thermally unstable, and isotopically anomalous presolar grains (A. Trinquier et al. 2009). In detail, since ^{46}Ti and ^{50}Ti originate from different nucleosynthetic sources, A. Trinquier et al. (2009) inferred that the correlated variations observed for these isotopes in meteorites are due to thermal processing rather than a coincidental consequence of the inhomogeneous distribution of the respective carrier phases in the early solar system. Likewise, T. Yokoyama et al. (2015) suggested that the ^{84}Sr and ^{54}Cr anomalies of solar system materials result from thermal processing and sublimation of ^{84}Sr and ^{54}Cr-enriched phases. In this scenario, NCs formed from the depleted residue, while CAI compositions record mixing between unprocessed CI-like material and gas enriched in the NR nuclides. Finally, the absence of W isotope anomalies and variations in the Mo isotope compositions of bulk meteorites have also been attributed to thermal processing and preferential loss of Mo, while more refractory W remained unaltered (C. Burkhardt et al. 2012).

Based on the correlation between the abundances of presolar grains and the extent of volatile depletion in CCs, G. R. Huss et al. (2003) suggested that both features were produced by thermal processing. Previous studies that examined the potential role of thermal processing in producing nucleosynthetic isotope anomalies focused on nonvolatile elements (A. Trinquier et al. 2009; W. Akram et al. 2015; C. Burkhardt & M. Schönbächler 2015; T. Yokoyama et al. 2015; M. Ek et al. 2020), which are mostly unaffected by volatile loss. In contrast, as a moderately volatile element, Zn has the potential for tracing both processes. Nonetheless, large variations in Zn concentrations are accompanied by indistinguishable nucleosynthetic Zn isotope compositions in bulk CCs, such that a direct correlation cannot be resolved (Figure 6(A)). This could, in principle, suggest decoupling between the processes responsible for the isotope anomalies and the variable Zn depletions.

Volatile element depletion in bulk CCs has been attributed to mixing between CI-like matrix and thermally processed, volatile-depleted components, including chondrules and refractory inclusions (E. Anders 1964; J. W. Larimer & E. Anders 1967; C. M. O. D. Alexander 2005, 2019a, 2019b; N. Braukmüller et al. 2018). This hypothesis is further supported by the observed correlations between mass-dependent isotope compositions and the abundances of some volatile elements in CCs, as these are consistent with mixing between an isotopically unfractionated CI-matrix and a fractionated and volatile-depleted nonmatrix component (NMC; J. L. Hellmann et al. 2020; N. X. Nie et al. 2021; E. M. Morton et al. 2024). Assuming that these characteristics were produced by thermal processing, it is conceivable that they could also be accompanied by distinct nucleosynthetic Zn isotope compositions for the NMC, resulting from preferential destruction of the carriers of the anomalous Zn. Coupled with variable mixing with a CI-like matrix, this scenario could possibly account for the nucleosynthetic Zn isotope variations of bulk chondrites.

Measured nucleosynthetic Zn isotope compositions for the various NMCs in chondrites are currently not available. Hence, to test this scenario, hypothetical Zn concentrations and nucleosynthetic isotope compositions of the NMCs were modeled for each meteorite group. To do so, a Monte Carlo simulation with 1000 trials was performed, where the bulk compositions of the CCs were calculated by mass balance assuming mixing between a CI-like matrix and the NMC. In each trial, the concentrations and nucleosynthetic Zn isotope compositions of bulk chondrites were generated within literature values (Table 7). The adopted CI-matrix fraction estimates for each group are from C. M. O. D. Alexander (2019a) and C. M. O. D. Alexander (2019b) but were renormalized to remove the water component (Table 7). The composition of the NMCs can then be modeled:

$$[Zn]_{bulk} = [Zn]_{matrix} \times F_{matrix} + [Zn]_{NMC} \times (1 - F_{matrix}) \quad (4)$$

and

$$\varepsilon^{64}Zn_{bulk} = \frac{\varepsilon^{64}Zn_{matrix} \times [Zn]_{matrix} \times F_{matrix} + \varepsilon^{64}Zn_{NMC} \times [Zn]_{NMC} \times (1 - F_{matrix})}{[Zn]_{matrix} \times F_{matrix} + \times [Zn]_{NMC} \times (1 - F_{matrix})}, \quad (5)$$

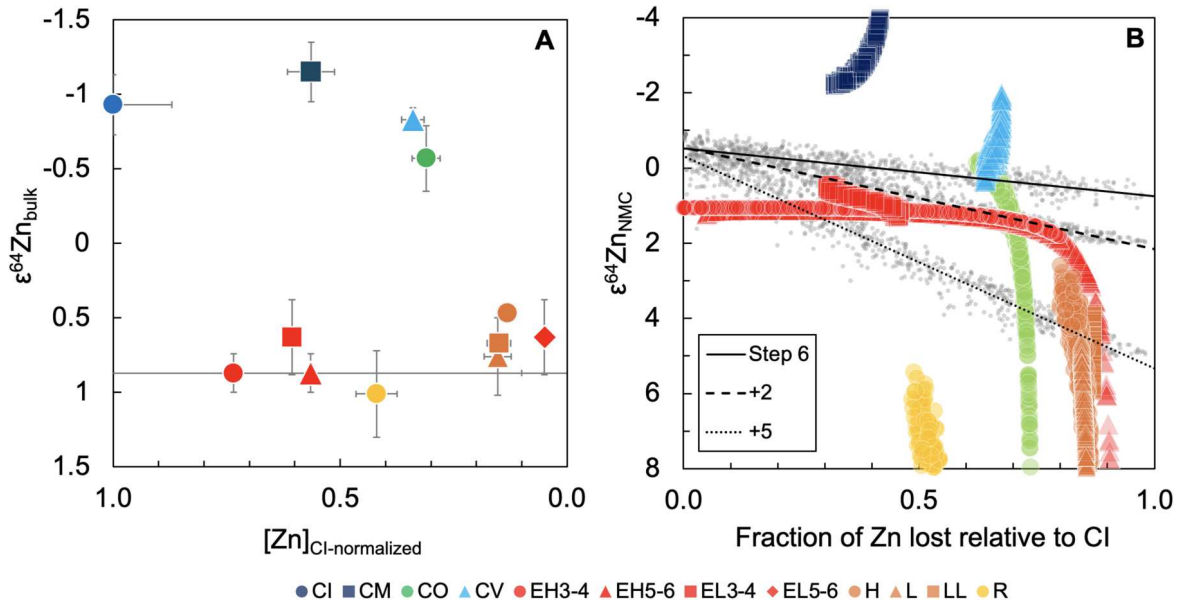


Figure 6. Variable nucleosynthetic Zn isotope compositions and Zn contents of bulk chondrites and their respective nonmatrix components (NMCs). (A) Plot of bulk ε^{64}Zn values vs. Zn concentrations normalized to CI values for the chondrites (Table 7). (B) Modelled ε^{64}Zn values for NMCs vs. bulk fraction of Zn lost. The results, shown as gray dots with lines corresponding to linear trends, were produced by Monte Carlo simulations (Equations (7)–(9)). The models assume a CI-like initial Zn isotope composition and concentration, and three different ε^{64}Zn values for the neutron-poor endmember: 0.61 ± 0.42 (Murchison Step 6; Run 1), 2.0 (Run 2), and 5.0 (Run 3). For comparison, the estimated compositions of the NMCs are shown as colored trends (Table 7; Equations (4)–(6)). Due to the highly variable Zn concentrations of ECs, EC3-4s and EC5-6s were treated separately. To maintain the focus on key results, some data for CM, CO, R, EH5-6, and L chondrites are not shown in the panel, as they exceed the *y*-axis scaling (Table 7). Note that the *y*-axes of both panels are flipped, in line with previous figures.

where F and [Zn] denote the material mass fraction and the Zn concentration of the materials, respectively. The fractions of Zn lost from the NMCs by thermal processing were also calculated for each trial:

$$f_{\mathrm{NMC_lost}} = 1 - \frac{[\mathrm{Zn}]_{\mathrm{NMC}}}{[\mathrm{Zn}]_{\mathrm{matrix}}}. \quad (6)$$

The Monte Carlo simulation results for the NMCs shown in brackets denote the minimum and maximum values obtained in all valid trials. Trials that yielded negative concentrations and fractions of Zn loss were excluded. Concentration data was compiled from N. Braukmüller et al. (2018), G. W. Kallemeyn et al. (1989, 1996), G. W. Kallemeyn & J. T. Wasson (1986), J. T. Wasson & G. W. Kallemeyn (1988), P. Kong et al. (1997), J. Isa et al. (2014), and H. Schulze et al. (1994). The nucleosynthetic Zn isotope results are from R. Martins et al. (2023) and R. Martins et al. (2024). Matrix fractions are from C. M. O. D. Alexander (2019a) and C. M. O. D. Alexander (2019b) but renormalized to remove water fractions.

The estimated compositions of the NMCs are typically neutron-poor (NP) and Zn-depleted compared to CIs (Table 7, Figure 6). The only exception is the CM group, which displays a mean nucleosynthetic Zn isotope composition that is more NR than that of CIs, resulting in a more NR composition for its NMC. This suggests that the NMCs of most chondrite groups would need to have preferentially lost Zn from the phases that host the NR Zn. As previously discussed, the NR Zn was likely originally hosted in presolar oxides or acid-resistant silicates attacked in Steps 4 and 5. In contrast, Step 6 is often relatively depleted in NR isotopes, either displaying indistinguishable compositions from the London Zn standard or even exhibiting NC-like isotope signatures (i.e., $\varepsilon^{64}Zn_{\mathrm{Murchison(6)}} = 0.61 \pm 0.42$). It is thus possible that Zn loss from the less-resistant phases attacked in Steps 1–5 could shift the bulk compositions toward complementary NC-like compositions that are dominated by NP Zn.

Notably, Steps 4 and 5 also released 90% of *all* Zn in Allende and Kainsaz (Tables 5 and 6; Figures 2 and 4). Hence, the carriers of the NR and of the bulk Zn are likely similar—if not identical. This resemblance potentially extends to the thermal susceptibilities of the phases, which would pose a challenge for isolating the NR Zn host phases by thermal processing. The fraction of Zn present in the most acid-resistant, NP components (<5%; Steps 6–7) is furthermore much lower than that hosted in the NR components of Steps 1–5 (>90%). Consequently, in order to attain NP compositions, substantial bulk Zn depletion is likely necessary.

Alternatively, it is possible that the NP component attacked in Step 6 was originally substantially more depleted in NR Zn isotopes compared to what is now observed even for the Step 6 leachate of Murchison. In this case, even limited loss of Zn from the NR Zn carriers can significantly impact the bulk Zn isotope compositions. The bulk-like compositions of Step 6 in some meteorites (i.e., $\varepsilon^{64}Zn_{\mathrm{Colony(6)}} = -0.70 \pm 0.26$) furthermore suggest that the minerals attacked in this step were also subjected to different extents of thermal homogenization. The original nucleosynthetic isotope composition of these acid-resistant phases is hence probably best preserved in the least thermally altered and most matrix-rich sample, Murchison. Nonetheless, phases with more extreme depletions in NR isotopes may have been originally present.

In either case, the compositions of the NMCs would reflect mixing between an NR, and an NP component, corresponding to Steps 1–5 and Step 6, respectively. To assess the feasibility of these different scenarios, three Monte Carlo simulations were performed, each for 1000 trials, in which the NP component was assigned a different composition for each run. As the Step 6 leachate for Murchison exhibits the largest observed depletions in isotopically anomalous Zn relative to

Table 7
Nucleosynthetic Zn Isotope Compositions, Zn Concentrations, and CI-Matrix Fractions Used in the Models, as Well as Estimated Zn Concentrations, Nucleosynthetic Zn Isotope Compositions, and Fractions of Zn Lost for the NMCs of Chondrites

Class	ε^{64}Zn	[Zn] (μg g^{-1})	F_{matrix} (%)	$[Zn]_{NMC}$	$\varepsilon^{64}Zn_{NMC}$	Zn Loss (%)
CI	−0.93 ± 0.20	312–391	100	…	…	…
CM	−1.15 ± 0.20	182–214	53.9	[0.1, 95.7]	[−47.62, −2.18]	[32, 46]
CO	−0.57 ± 0.22	100–119	25.2	[2.1, 52.3]	[−0.21, 24.33]	[62, 74]
CV	−0.83 ± 0.08	112–127	26.0	[34.2, 41.7]	[−1.97, 0.35]	[64, 68]
EH 3-4	0.87 ± 0.13	62–450	7.5	[42.2, 375.9]	[1.06, 1.82]	[0, 80]
EH 5-6	…	21–372	7.5	[0, 370.0]	[−75.89, 427.5]	[5, 93]
EL 3-4	0.63 ± 0.25	209–218	8.0	[194.0, 209.6]	[0.44, 1.34]	[30, 46]
EL 5-6	…	13–22	8.0	…	…	…
H	0.47 ± 0.04	41–51	10.0	[10.9, 13.2]	[3.87, 5.94]	[86, 87]
L	0.76 ± 0.26	44.5–63	11.3	[2.2, 30.9]	[2.60, 37.53]	[80, 88]
LL	0.67 ± 0.02	41–60.6	11.6	[10, 17.2]	[4.55, 8.34]	[85, 86]
R	1.01 ± 0.29	134–162	36.5	[2.1, 74.0]	[5.43, 194.12]	[49, 66]

the bulk composition, $\varepsilon^{64}Zn_{NP}$ for Run 1 was assigned randomly generated values in a normal distribution within twice the standard deviation of the mean result obtained for this leaching step ($\varepsilon^{64}Zn_{NP} = 0.61 \pm 0.42$). For the two remaining runs, this component was assigned more extreme values, corresponding to $\varepsilon^{64}Zn_{NP} = 2.0$ and 5.0, for Runs 2 and 3, respectively.

In all three runs, the Zn isotope compositions of the complementary NR components were generated with a normal distribution, varying within twice the standard deviation of the mean ε^{64}Zn values determined for Steps 1–5 of the four analyzed chondrites ($\varepsilon^{64}Zn_{NR} = -0.83 \pm 0.29$, 2sd; each leach step was thereby weighted by the Zn fraction it contributed to the total Zn mass present in Steps 1–5 of a given chondrite). Even though Steps 1–3 are unlikely to be the original carriers of the NR Zn, they were included in the NR component, as they are more labile and would also possibly be destroyed at the conditions that are required to thermally process the minerals attacked in Steps 4 and 5. In addition, their compositions mostly overlap with those of Steps 4 and 5. Finally, the Zn contributions of Step 7 were relatively minor for all chondrites (0.8% Zn fraction on average), and its composition was indistinguishable from the bulk values of all four meteorites. The effects of this component on the final compositions are therefore likely negligible, and it was hence not included in the model.

Assuming that they result in a CI-like composition, the initial fractions of the NR and NP components prior to thermal processing can be modeled by mass balance:

$$\varepsilon^{64}Zn_{CI-matrix} = \varepsilon^{64}Zn_{NP} \times f_{NP_initial} + \varepsilon^{64}Zn_{NR} \times f_{NR_initial}. \quad (7)$$

Here, $f_{NP_initial}$ and $f_{NR_initial}$ refer to the initial fractions of Zn in each component, before Zn loss from the NR component, and with $f_{NP_initial} + f_{NR_initial} = 1$. The fraction of Zn lost from the NR component (f_{NR_lost}) was randomly generated in each trial and allowed to vary between 0% and 100%. This was used to calculate the remaining Zn fractions of the NR and NP components (Equation (8)), with $f_{NP_final} + f_{NR_final} = 1$. The composition of the NMC after preferential loss of Zn from the NR component can then be calculated (Equation (9))

$$f_{NR_{final}} = f_{NR_{initial}} \times (1 - f_{NR_{lost}}) \quad (8)$$

$$\varepsilon^{64}Zn_{NMC} = \varepsilon^{64}Zn_{NP} \times f_{NP_final} + \varepsilon^{64}Zn_{NR} \times f_{NR_final}. \quad (9)$$

The results of all three runs of the thermal processing model are shown in Figure 6. Some of the modeled NMC_{CV} compositions overlap with the results from Run 1 of the thermal processing model, which were obtained with an NP component defined by the Step 6 Murchison leachate (Figure 6, Table 7). The Run 1 trend is furthermore compatible with some of the calculated NMC_{CO} values. The NMC_{CO} composition is, however, also in accord with the Run 2 and 3 results, as a consequence of the larger uncertainty of the nucleosynthetic Zn isotope composition of COs and therefore of NMC_{CO}. Finally, as bulk CMs are more NR than the CI-matrix, none of the model runs can account for the NMC_{CM} composition (Figure 6, Table 7).

In contrast, the NMC_R requires a much more extreme depletion in NR Zn compared to what is achieved in any of the Runs (Figure 6, Table 7). This is because R chondrites display the most NP compositions among the available chondrites while showing a relatively limited Zn depletion. However, the compositions of the other NC groups are largely consistent with the thermal processing models. In detail, the three OC groups require similar characteristics for their NMCs, some of which can be reconciled with Run 3, but most of the trials require neutron-poorer compositions (Figure 6, Table 7). The large range of the EH bulk Zn concentrations propagates into large uncertainties for the estimated NMC compositions, which are, hence, compatible with the results of both Runs 2 and 3. With a much narrower range of Zn concentrations, the EL3-4 NMC values are compatible with Run 2 (Figure 6, Table 7). However, the NMC compositions of EL5-6 chondrites could not be modeled, as they require negative Zn concentrations for the quoted matrix fraction to offset the low bulk Zn contents.

Notable in this context is that ECs have highly variable concentrations of Zn and other volatile elements, and this variability may not be an original feature but a consequence of secondary processes (G. W. Kallemeyn & J. T. Wasson 1986; F. Moynier et al. 2011; C. Palk et al. 2018). This is supported by the Te isotope systematics of ECs, which have been interpreted as resulting from mobilization of Te from the parent body interiors (the source of EC5-6s) and subsequent Te recondensation in the exterior layers from where the EC3-4s are derived (J. L. Hellmann et al. 2021). If this process can be extended to other moderately volatile elements, it is conceivable that the bulk Zn concentrations of the EC parent

bodies are intermediate between the EC3-4 and EC5-6 abundances. If the latter interpretation is correct, the revised modeled NMC compositions of the ECs would likely be consistent with either the Run 2 or Run 3 results, or an intermediate composition.

In summary, the modeling suggests that the nucleosynthetic Zn isotope compositions and concentrations of bulk chondrites can largely be reproduced by preferential Zn loss from the more labile phases that host NR Zn in thermally processed nonmatrix material, in accord with the results of the leaching experiments. However, the compositions of (1) COs and CVs are most compatible with the Run 1 results; (2) ECs are in accord with the results of Runs 2 or 3; and (3) some OC results can be reconciled with Run 3. Furthermore, CM and R chondrites have compositions that are incompatible with any of the runs. As such, no single composition for the NP component can account for the bulk compositions of the different chondrite groups by varying only the extent of Zn loss. Instead, different compositions for the NP component are required depending on the group. This would imply that chondrites incorporated heterogeneous materials, which may be sampled not only by their NMC, but also by their matrix. However, such a scenario can directly account for the variable observed Zn isotope compositions and concentration of bulk chondrites, rendering thermal processing and preferential loss of certain carrier phases unnecessary.

As an alternative to thermal processing, variations in nucleosynthetic isotope compositions can also be achieved if the molecular cloud from which the protoplanetary disk formed was never fully homogenized (N. Dauphas et al. 2002). This could reflect either periodic episodes of accretion in the protoplanetary nebula, with the composition of the infalling molecular cloud material varying over time, or uneven distribution of presolar dust across the solar system (P. H. Warren 2011; J. A. M. Nanne et al. 2019). The formation of Jupiter is also hypothesized to have played a role, by acting as an effective barrier preventing mixing between the inner and outer solar system (T. S. Kruijer et al. 2017). These scenarios can account for NC compositions that are depleted in NR isotopes from explosive nucleosynthesis and CCs that are enriched in NR nuclides, in accord with the Zn isotope results (R. Martins et al. 2023, 2024).

5. Conclusions

Sequential acid-leaching of CCs revealed the presence of isotopically anomalous, NR Zn, with negative ε^{64}Zn and positive ε^{68}Zn and ε^{70}Zn relative to a terrestrial standard, in all chondrites. However, the distribution of this Zn between the different leaching steps varied between the meteorites. This implies variable isotopic homogenization between different mineral phases, such that the anomalous Zn is no longer hosted solely in its original carrier phase. The compositions of the different leachate fractions were most commonly identical to those of the bulk meteorites, with the largest isotope anomalies present in oxide/silicate-attacking steps. This suggests that the anomalous Zn was most likely initially hosted in oxides or acid-resistant silicates derived from explosive nucleosynthesis in either SNe Ia or ECSNe.

The leaching steps that carried the largest mass fractions of isotopically anomalous, NR Zn also contained most of the total Zn inventory (Steps 4–5), with the first HF step yielding about 90% of the total Zn budget for three of the four meteorites (Step 4). The single exception is Murchison, where most of the Zn is likely hosted in aqueous alteration products (Step 1). As such, the presolar carriers of the NR Zn are similar or possibly identical to the mineral phases that initially hosted the bulk of the CC Zn inventories. This similarity renders it unlikely that the carrier phases of the NR Zn can be separated from the phases that predominantly host the Zn budgets of CCs by physical mechanisms such as thermal processing.

An alternative scenario follows from the finding that the more acid-resistant components leached in Step 6 initially had NP, NC-like Zn isotope compositions, as observed for Murchison. Given this, substantial loss of Zn from the more labile minerals attacked in Steps 1–5 could potentially produce nucleosynthetic Zn isotope anomalies. However, modeling revealed that no single composition for the acid-resistant component depleted in NR nuclides can produce the variations in Zn concentrations and isotope compositions observed for chondrites solely through variable loss of anomalous, NR Zn. Instead, different chondrite groups require distinct compositions for the NP component. Such a scenario can, however, directly explain the anomalies without the need for thermal processing and preferential destruction of an exotic component.

In summary, the constraints presented in this study suggest that thermal processing alone cannot account for the mass-independent Zn isotope variations observed for chondrites. While such mechanisms may have contributed, the observed heterogeneities may solely be a consequence of temporal and spatial changes in the composition of the molecular cloud followed by restricted mixing between the CC and NC reservoirs. Future studies would benefit from improved constraints on the Zn concentrations of some chondritic meteorites, particularly ECs, as well as leaching studies of less thermally altered/more matrix-rich samples, such as CIs.

Acknowledgments

We are grateful to the Russian Academy of Sciences and the Smithsonian Institution for providing the meteorite samples, Jens Barosch for logistic support, and Carsten Münker for lab use in Cologne. This work was funded by an Imperial College London President's PhD Scholarship (R.M.), ERC grants 101020665 (R.M., H.M.W.) and 669666 (A.B., C.M.), and UKRI STFC grant ST/W001179/1 (M.R., E.M.M.). We thank Tim Elliott and Matt Genge for constructive comments on an early version of the manuscript.

ORCID iDs

Rayssa Martins https://orcid.org/0000-0003-2453-5942
Elin M. Morton https://orcid.org/0000-0001-6208-2388

References

Akram, W., Schönbächler, M., Bisterzo, S., & Gallino, R. 2015, GeCoA, 165, 484
Alexander, C. M. O. D. 2005, M&PS, 40, 943
Alexander, C. M. O. D. 2019a, GeCoA, 254, 277
Alexander, C. M. O. D. 2019b, GeCoA, 254, 246
Anders, E. 1964, SSRv, 3, 583
Bragagni, A., Wombacher, F., Kirchenbaur, M., Braukmüller, N., & Münker, C. 2023, GeCoA, 344, 40
Braukmüller, N., Wombacher, F., Hezel, D. C., Escoube, R., & Munker, C. 2018, GeCoA, 239, 17
Bridgestock, L. J., Williams, H., Rehkämper, M., et al. 2014, E&PSL, 400, 153

Budde, G., Burkhardt, C., & Kleine, T. 2019, NatAs, 3, 736
Burkhardt, C., Kleine, T., Dauphas, N., & Wieler, R. 2012, E&PSL, 357, 298
Burkhardt, C., & Schönbächler, M. 2015, GeCoA, 165, 361
Dauphas, N., Chen, J. H., Zhang, J., et al. 2014, E&PSL, 407, 96
Dauphas, N., Marty, B., & Reisberg, L. 2002, ApJ, 565, 640
Ek, M., Hunt, A. C., Lugaro, M., & Schonbachler, M. 2020, NatAs, 4, 273
Fischer-Gödde, M., & Kleine, T. 2017, Natur, 541, 525
Heger, A., Fröhlich, C., & Truran, J. W. 2014, in Treatise on Geochemistry (Second Edition), ed. H. D. Holland & K. K. Turekian (Oxford: Elsevier), 1
Hellmann, J. L., Hopp, T., Burkhardt, C., & Kleine, T. 2020, E&PSL, 549, 116508
Hellmann, J. L., Hopp, T., Burkhardt, C., et al. 2021, GeCoA, 309, 313
Huss, G. R., Meshik, A. P., Smith, J. B., & Hohenberg, C. M. 2003, GeCoA, 67, 4823
Isa, J., Rubin, A. E., & Wasson, J. T. 2014, GeCoA, 124, 131
Kallemeyn, G. W., Rubin, A. E., Wang, D., & Wasson, J. T. 1989, GeCoA, 53, 2747
Kallemeyn, G. W., Rubin, A. E., & Wasson, J. T. 1996, GeCoA, 60, 2243
Kallemeyn, G. W., & Wasson, J. T. 1986, GeCoA, 50, 2153
King, A. J., Henkel, T., Rost, D., & Lyon, I. C. 2012, M&PS, 47, 1624
King, A. J., Schofield, P. F., & Russell, S. S. 2017, M&PS, 52, 1197
Kong, P., Mori, T., & Ebihara, M. 1997, GeCoA, 61, 4895
Krot, A. N., Keil, K., Scott, E. R. D., Goodrich, C. A., & Weisberg, M. K. 2014, in Treatise on Geochemistry (Second Edition), ed. H. D. Holland & K. K. Turekian (Oxford: Elsevier), 1
Kruijer, T. S., Burkhardt, C., Budde, G., & Kleine, T. 2017, PNAS, 114, 6712
Larimer, J. W., & Anders, E. 1967, GeCoA, 31, 1239
Lodders, K. 2003, ApJ, 591, 1220
Lodders, K., & Amari, S. 2005, ChEG, 65, 93
Luck, J.-M., Ben Othman, D., & Albarède, F. 2005, GeCoA, 69, 5351
Lugaro, M. 2005, Stardust from Meteorites, Vol. 9 (Singapore: World Scientific)
Martins, R., Kuthning, S., Coles, B. J., Kreissig, K., & Rehkämper, M. 2023, Sci, 379, 369
Martins, R., Morton, E. M., Kuthning, S., et al. 2024, SciA, 10, eado4121
Morton, E. M., Pickard, H., Wombacher, F., et al. 2024, ApJ, 977, 53
Moynier, F., Paniello, R. C., Gounelle, M., et al. 2011, GeCoA, 75, 297
Nanne, J. A. M., Nimmo, F., Cuzzi, J. N., & Kleine, T. 2019, E&PSL, 511, 44
Nie, N. X., et al. 2021, SciA, 7, eabl3929
O'Neill, H. S. C. 1991, GeCoA, 55, 1159
Palk, C., Andreasen, R., Rehkämper, M., et al. 2018, M&PS, 53, 167
Palme, H., & Mezger, K. 2024, M&PS, 59, 382
Qin, L., Carlson, R. W., & Alexander, C. M. O. D. 2011, GeCoA, 75, 7806
Robinson, P. 2025, GGRes, 49, 9
Rotaru, M., Birck, J. L., & Allègre, C. J. 1992, Natur, 358, 465
Rubin, A., Trigo-Rodríguez, J. M., Huber, H., & Wasson, J. T. 2007, GeCoA, 71, 2361
Rubin, A., & Ma, C. 2021a, Meteorite Mineralogy: Mineralogy of Major Physical Components of Chondrites (Cambridge: Cambridge Univ. Press), 109
Rubin, A., & Ma, C. 2021b, Meteorite Mineralogy: Petrologic and Mineralogical Characteristics of Meteorite Groups (Cambridge: Cambridge Univ. Press), 109
Rüfenacht, M., Morino, P., Lai, Y.-J., et al. 2023, GeCoA, 355, 110
Savage, P. S., Moynier, F., & Boyet, M. 2022, Icar, 386, 115172
Schulze, H., Bischoff, A., Palme, H., et al. 1994, Metic, 29, 275
Steller, T., Burkhardt, C., Yang, C., & Kleine, T. 2022, Icar, 386, 115171
Taylor, G. J. 2013, ChEG, 73, 401
Torrano, Z. A., Brennecka, G. A., Williams, C. D., et al. 2019, GeCoA, 263, 13
Trinquier, A., Birck, J. L., & Allegre, C. J. 2007, ApJ, 655, 1179
Trinquier, A., Elliott, T., Ulfbeck, D., et al. 2009, Sci, 324, 374
Wanajo, S., Janka, H.-T., & Müller, B. 2013, ApJL, 767, L26
Warren, P. H. 2011, E&PSL, 311, 93
Wasson, J. T., & Kallemeyn, G. W. 1988, RSPTA, 325, 535
Woosley, S. E. 1997, ApJ, 476, 801
Yokoyama, T., Fukami, Y., Okui, W., Ito, N., & Yamazaki, H. 2015, E&PSL, 416, 46
Yokoyama, T., & Tsujimoto, T. 2021, in Encyclopedia of Geology (Second Edition), ed. D. Alderton & S. A. Elias (Oxford: Academic Press)